

NEUROSCIENCE

A global screen for magnetically induced neuronal activity in the pigeon brain

Gregory C. Nordmann^{1,2,3,†}, Spencer D. Balay^{1,3,†},
Thamari N. Kapurige^{1,4}, Marco Numi¹, Christoph Leeb⁵,
Simon Nimpf¹, E. Pascal Malkemper⁶, Lukas Landler⁷,
David A. Keays^{1,8,9*}

How animals detect Earth's magnetic field remains a mystery in sensory biology. Despite extensive behavioral evidence, the neural circuitry and molecular mechanisms responsible for magnetic sensing remain elusive. Adopting an unbiased approach, we used whole-brain activity mapping, tissue clearing, and light sheet microscopy to identify neuronal populations activated by magnetic stimuli in the pigeon (*Columba livia*). We demonstrate robust, light-independent bilateral neuronal activation in the medial vestibular nuclei and the caudal mesopallium. Single-cell RNA sequencing of the semicircular canal cristae revealed specialized type II hair cells that express the molecular machinery necessary for the detection of magnetic stimuli by electromagnetic induction. Our data support a model whereby electromagnetic input from the semicircular canals activates a vestibular-mesopallial circuit in the pigeon brain.

How animals detect and respond to magnetic fields has perplexed scientists for more than a century. Although behavioral studies have provided compelling evidence for the existence of a magnetic sense, the molecules, cells, and central circuits involved in magnetoreception are unknown. To date, three putative transduction mechanisms have been proposed: magnetoreception based on the iron oxide magnetite (1, 2); a light-dependent mechanism that relies on the formation of spin-correlated radical pairs in cryptochrome molecules (3); and electromagnetic induction mediated by voltage-sensitive ion channels (4). Each of these mechanisms has been associated with a putative anatomical location. It has been suggested that magnetite-based magnetoreceptors are associated with trigeminal neurons (5, 6); light-dependent sensors are believed to reside in the retina (7, 8); and electromagnetic induction could occur within the inner ear (9).

Following the detection of the stimulus in the periphery, it has been proposed that magnetosensory information is transmitted to the brain via distinct cranial nerves (10, 11). Our understanding of the central circuits that process magnetic information is limited because previous studies have largely relied on histological sections to assess neuronal activity in candidate brain structures. These studies have implicated a region of the visual Wulst called cluster N (12), the trigeminal brainstem complex (6), and the vestibular nuclei in the processing of magnetic information in birds (13). Most investigations have been driven, but also biased by, the hypotheses that they seek to test. This is problematic

because magnetic fields penetrate all organic material and therefore the primary sensors could be anywhere; and animals may have evolved distinct neuronal circuits dedicated to the processing and integration of magnetic information. We resolved to take an unbiased top-down approach to study magnetosensation. We reasoned that screening the entire pigeon brain for sensory-driven neuronal activity in a systematic and unsupervised manner would enable the identification of magnetically activated neuronal populations, which in turn would inform our search for the primary magnetosensors. We therefore developed a pipeline for whole-brain analysis of immediate early genes (IEGs) in *Aves* that exploits advances in whole-brain clearing and light sheet microscopy.

A pipeline to screen the pigeon brain for sensory circuits

To define magnetically activated neurons in the pigeon, we adapted an IEG detection pipeline that is based on the iDISCO neuronal mapping paradigm (Fig. 1A) (14). First, we optimized tissue clearing for the pigeon brain, adjusting the iDISCO protocol to account for the large volume and cytoarchitectural properties of the avian pallium while maintaining tissue transparency and morphology with moderate isotropic shrinkage (Fig. 1, B and C). We coupled this clearing protocol with fluorescent labeling of the IEG C-FOS and developed a light sheet imaging procedure to visualize an entire hemisphere of the pigeon brain at single-cell resolution (Fig. 1D and fig. S1). To analyze whole-brain C-FOS data, we adapted the open-source tool ClearMap to a common reference coordinate system for the pigeon brain, permitting identification of differentially activated brain regions (Fig. 1, D and E). To address issues associated with multiple testing, we implemented a permutation-based shuffling procedure to determine a minimum cluster-size threshold when analyzing C-FOS clusters (15) (fig. S2).

To ascertain whether our pipeline could be used to identify sensory circuits in the pigeon brain, we performed a proof-of-concept experiment using an auditory stimulus where the neuronal circuits are defined (16). Birds ($n = 6$ animals) were exposed to high-frequency sounds (2 to 10 kHz) for 60 min, while a control group received no auditory input (Fig. 1F). Fixed brains were stained, cleared, imaged, and C-FOS⁺ cells were quantified using ClearMap. This revealed an enrichment of C-FOS⁺ cells in known anatomical loci of the pigeon ascending auditory pathway in those birds exposed to sound (Fig. 1G). For example, clusters of activated voxels were observed in the secondary cochlear nucleus laminaris, where sound stimulation resulted in a significant increase in C-FOS⁺ cells ($P < 0.05$, $t = 3.170$; Fig. 1, H to K); in the superior olive (SO) ($P < 0.01$, $t = 3.939$; Fig. 1, L to N); and in the nucleus mesencephalicus lateralis, pars dorsalis (MLD) ($P < 0.005$, $t = 5.016$; Fig. 1, O to Q).

Magnetic activation in the light

Next, we coupled our screening pipeline to established magnetic stimuli to define the central magnetosensory circuit in pigeons (4, 13). Under white light (400 to 700 nm), head-fixed animals ($n = 13$) were exposed to a rotating 150 μ T magnetic field stimulus for 72 min, while control animals ($n = 13$) received no magnetic input (Fig. 2A). We screened for magnetically induced C-FOS expression, initially focusing on regions of the brain innervated by cranial nerves known to carry peripheral sensory information (Fig. 2A). Magnetic fields did not induce C-FOS expression in the primary nuclei of the olfactory (Fig. 2B), visual (Fig. 2, C and D), trigeminal (Fig. 2E), facial (Fig. 2E), auditory (Fig. 2F), glossopharyngeal (Fig. 2G), or vagal (Fig. 2G) systems. In contrast, we observed large clusters of significantly activated voxels in the caudal medial vestibular nucleus (VeM), a structure innervated by the vestibulocochlear nerve (17) (Fig. 2H). These activated clusters were bilateral and overlapped with C-FOS densities reported in previous histological experiments (4, 13). Count extraction from the activated VeM voxels revealed a 90% increase in C-FOS⁺ cells in the treatment group in comparison to controls ($P < 0.01$, $t = 3.637$; Fig. 2I). We also observed large bilateral clusters of activation in the caudal mesopallium, a region of the pallium associated with multisensory integration

¹Department of Biology, Ludwig-Maximilians-University (LMU) Munich, Planegg-Martinsried, Germany. ²Max Planck Institute for Biological Intelligence, Planegg-Martinsried, Germany. ³Vienna Biocenter PhD Program, a Doctoral School of the University of Vienna and the Medical University of Vienna, Vienna, Austria. ⁴Graduate School of Systemic Neurosciences, Planegg-Martinsried, Germany. ⁵Herpetological Collection, Natural History Museum Vienna, Vienna, Austria. ⁶Max Planck Institute for Neurobiology of Behavior – caesar, Bonn, Germany. ⁷Institute of Zoology, BOKU University, Vienna, Austria. ⁸Department of Physiology, Development and Neuroscience, University of Cambridge, Cambridge, UK. ⁹Research Institute of Molecular Pathology (IMP), Vienna Biocenter (VBC), Vienna, Austria. *Corresponding author. Email: keays@bio.lmu.de †These authors contributed equally to this work.

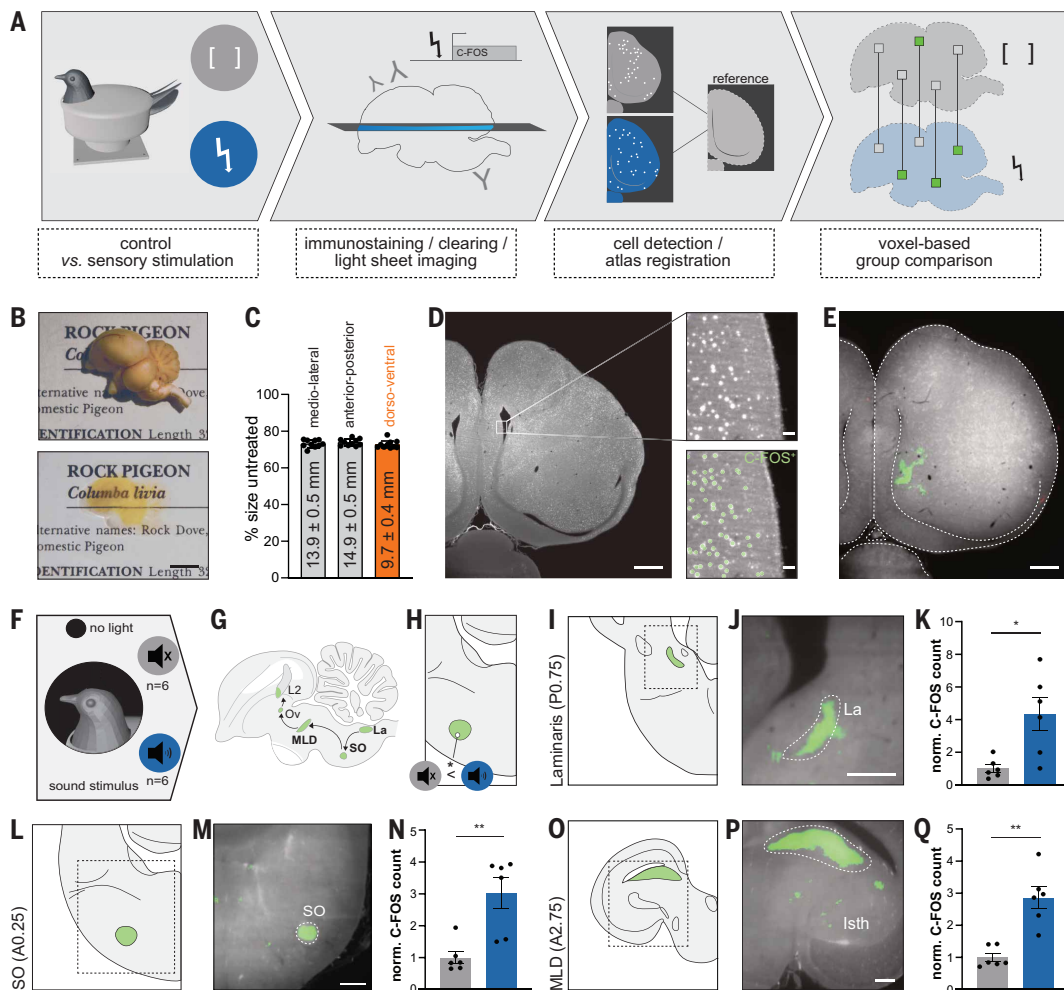


Fig. 1. A pipeline to screen for sensory-induced neuronal activity in pigeon brains. (A) Overview of the activity mapping pipeline. Restrained birds received no sensory input (gray) or sensory stimulation (blue). Brains were stained for C-FOS, cleared, and imaged. C-FOS⁺ cells were detected, and image stacks were analyzed with ClearMap. (B) Pigeon brain before and after iDISCO. (C) Clearing-induced shrinkage of pigeon brains is isotropic. (D) Optical section of the pigeon brain (horizontal). Single-cell resolution (top right panel) allows the automated detection of C-FOS⁺ cells (green dots). (E) *P*-value maps (green voxels) are overlaid with the reference template to localize areas of differential C-FOS expression. (F) Proof-of-principle auditory experiment. Pigeons ($n = 6$) were exposed to no sound (gray) or high-frequency sounds (blue). (G) Nuclei in the ascending auditory pathway include the nucleus laminaris (La), the superior olive (SO), and the nucleus mesencephalicus lateralis, pars dorsalis (MLD). (H) Green pixels depict voxels with a significant ($P < 0.05$) increase in C-FOS density. (I to Q) Sound exposure resulted in C-FOS enrichment in the cochlear nucleus laminaris [(I) to (K)], superior olive [(L) to (N)], and MLD [(O) to (Q)]. Panels show a coronal section of the pigeon brain atlas with the region of interest highlighted in green on the left, the *P*-value map overlaid with a coronal reconstruction of the template brain in the center, and the normalized C-FOS densities of the control (gray) and stimulus (blue) group on the right. Bars represent mean \pm SEM. * $P < 0.05$, ** $P < 0.01$; two-tailed *t* test after Bonferroni correction. Scale bars: (B) 5 mm, (D) 1 mm and 50 μ m (insets), (E) 1 mm, and [(J), (M), and (P)] 500 μ m.

(18) (Fig. 2J). Here, there was a 30% increase in C-FOS⁺ cells compared to controls ($P < 0.005$, $t = 3.951$; Fig. 2K). Activated clusters lined the hippocampal ventricle and were medial of the auditory field L2 region (L2). Farther anterior (A8.25), the dorsomedial hippocampus showed a 30% increase in C-FOS counts after magnetic stimulation ($P < 0.05$, $t = 3.282$; Fig. 2, L and M). We did not observe significant activation associated with a proposed magnetic trigeminal circuit in the ventral principal sensory trigeminal nucleus (PrV) (Fig. 2E), the telencephalic frontal nidopallium (NFT), or the nucleus basalis (Bas) (19) (fig. S3, D to F). Total C-FOS counts extracted from the whole brain were not increased in animals exposed to magnetic stimuli ($P > 0.9$, $t = 0.1264$; Fig. 2, N and O), indicating that exposure to magnetic fields does not lead to a global increase in neuronal activity but instead activates specific neuronal populations.

Magnetic activation in the dark

There is evidence that migratory birds detect magnetic fields by relying on a light-dependent magnetoreceptor that resides in the retina

and is dependent on afferent thalamofugal visual circuits and a region of the avian forebrain referred to as cluster N (12). It is conceivable that such a magnetosensitive system could exist in pigeons and result in downstream activation within the vestibular system, which might explain the activation we observed in VeM. To test this, we repeated the aforementioned experiment in total darkness ($n = 14$ animals) (Fig. 3A). We again screened the cranial nerve input stations to determine whether magnetic stimulation in the dark activated any regions known to receive primary sensory information. Magnetic stimuli did not induce C-FOS expression in the olfactory (Fig. 3B), visual (Fig. 3, C and D), trigeminal (Fig. 3E), facial (Fig. 3E), auditory (Fig. 3F), glosopharyngeal (Fig. 3G), or vagal (Fig. 3G) systems. The VeM again showed large bilateral clusters of activated voxels after exposure to magnetic stimulation. Here, C-FOS⁺ counts were increased by 69% in comparison to controls ($P < 0.05$, $t = 2.936$; Fig. 3, H and I). The VeM projects to the superior vestibular nucleus (VeS), the vestibulocerebellum, and the dorsal thalamus (20). While we did not observe magnetic

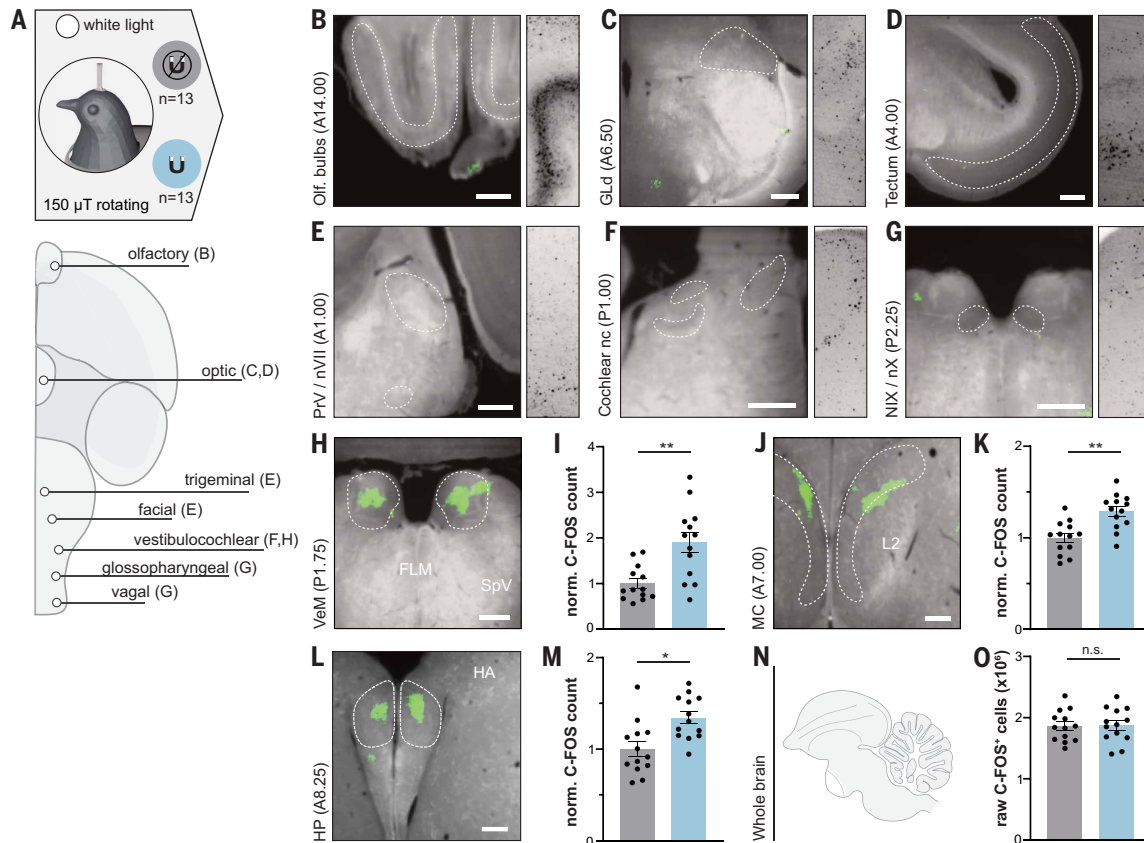


Fig. 2. Magnetic activation under white light. (A) Birds were exposed to either a zero magnetic field (gray) or a rotating 150 μT magnetic stimulus (blue) for 72 min under white light (400 to 700 nm) in a magnetically shielded room ($n = 13$). (Bottom) Ventral view of the pigeon brain highlighting the cranial nerves that transmit sensory information. (B to G) P -value anatomical maps of cranial nerve input stations. Right-hand insets show raw C-FOS staining. No significant clusters (green voxels) were found in the (B) olfactory bulbs, (C) nucleus geniculatus pars dorsalis (GLd), (D) optic tectum, (E) principal sensory trigeminal nucleus (PrV), (F) facial (nVII), (G) cochlear nuclei, or (G) glossopharyngeal/vagal nuclei (NIX/nx). (H to M) Activated clusters were observed in the caudal medial vestibular nuclei (VeM) [(H) and (I)], in the caudal mesopallium (MC) [(J) and (K)], and in the anterior dorsomedial hippocampus (HP) [(L) and (M)]. (N and O) Whole-brain C-FOS counts reveal no difference between the two groups. Bar plots represent the mean \pm SEM. C-FOS counts were normalized to the control group. * $P < 0.05$, ** $P < 0.01$; two-tailed t test after Bonferroni correction. Scale bars: 500 μm . FLM, fasciculus longitudinalis medialis; SpV, spinal trigeminal sensory nucleus; L2, field L2; HA, hyperpallium apicale.

activation in the VeS or cerebellum, we found bilateral clusters of activation in the dorsomedial thalamus (DTh) within the anterior dorsomedial nucleus (DMA) ($P < 0.01$, $t = 3.643$; Fig. 3, M and N, and fig. S4). Further analysis of our dark dataset again revealed large activation clusters in the mesopallium that spanned from the caudal pole (A7.00) to the medial intermedioventral subdivision (A11.00). Quantification revealed a 57% increase in C-FOS⁺ cells in birds exposed to magnetic fields ($P < 0.01$, $t = 3.573$; Fig. 3, J and K). Additionally, neuronal activation was evident in the left dorsomedial hippocampus (A7.00), where C-FOS⁺ cells were increased by 65% in the magnetically stimulated group ($P < 0.01$, $t = 3.470$; Fig. 3, O and P). Total C-FOS counts in the entire brain of experimental and control birds were again similar ($P > 0.5$, $t = 0.8675$; Fig. 3L).

We performed an overlap analysis of the activated voxels between light and dark P -value maps (fig. S5A). Anatomical assignment revealed two loci of shared activation: the VeM (fig. S5, B to D) and the caudal mesopallium (fig. S5, E to G). As we have previously reported magnetically induced activation in the VeM, we set out to replicate the activation observed in the caudal mesopallium in a third set of animals by traditional histology (4). We observed a significant increase in C-FOS density within the overlapping region of the caudal mesopallium in birds exposed to a rotating 150 μT stimulus protocol in both the light and dark ($P < 0.01$, $F = 8.032$; fig. S6). To gain further insight into the

underlying biophysical mechanisms, we then asked whether a static magnetic field would be sufficient to induce C-FOS expression in the pigeon brain. Although it is conceivable that a static field could activate magnetite-based magnetoreceptors, a changing magnetic field is a prerequisite for electromagnetic induction to occur (9). We exposed birds to either (i) a null magnetic field or (ii) a static 150 μT magnetic field ($n = 12$) (fig. S7A). We observed no C-FOS enrichment in the vestibular nuclei ($P > 0.5$, $t = 0.3259$; fig. S7, B and C), mesopallium ($P > 0.5$, $t = 0.3763$; fig. S7, D and E), dorsal thalamus ($P > 0.5$, $t = 0.9190$; fig. S7, G and H), or hippocampus ($P > 0.5$, $t = 1.088$; fig. S7, I and J) in birds exposed to a 150 μT static field. Whole-brain C-FOS counts were again similar when comparing groups ($P > 0.5$, $t = 0.3555$; fig. S7F).

The molecular profile of the vestibular ampullae

The vestibular nuclei are innervated by the vestibulocochlear nerves, which receive input from the utricle, saccule, and lagena (which detect gravity) and the semicircular canals (which detect angular momentum) (17). Given that extensive investigation has failed to identify magnetite within these structures (21, 22) and that changing magnetic field is required for C-FOS activation, we focused on the semicircular canals where electromagnetic induction could occur. At the base of each semicircular canal lies the crista ampullaris, which consists of a

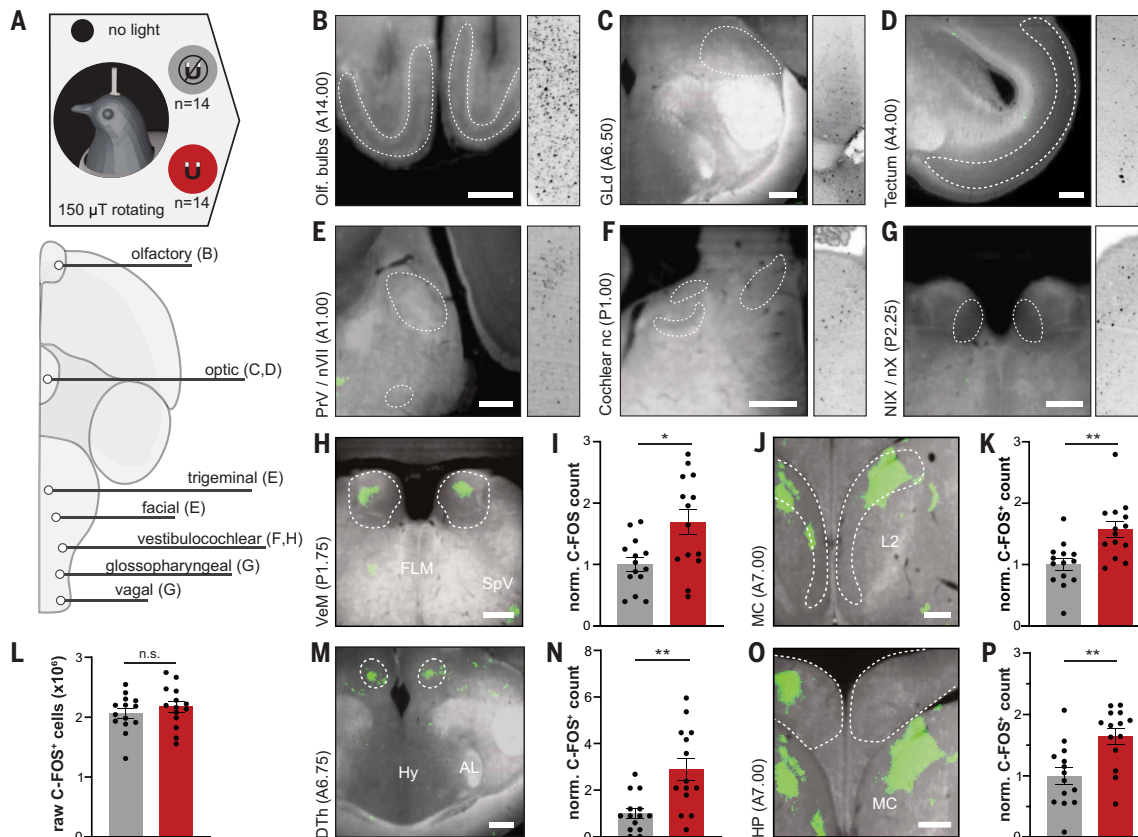


Fig. 3. Magnetic activation in the dark. (A) Birds were exposed to either a zero magnetic field (gray) or a rotating 150 μT magnetic stimulus (red) for 72 min in total darkness within a magnetically shielded room ($n = 14$). (Bottom) Ventral view of the pigeon brain highlighting the cranial nerves that transmit sensory information. (B to G) P -value anatomical maps of cranial nerve input stations. Right-hand insets show raw C-FOS staining. No significant clusters (green voxels) were observed in the (B) olfactory bulbs, (C) nucleus geniculatus pars dorsalis (GLd), (D) optic tectum, (E) principal sensory trigeminal nucleus (PrV), (E) facial (nVII), (F) cochlear nuclei, or (G) glossopharyngeal/vagal nuclei (NIX/nX). Activated C-FOS clusters were observed in (H and I) the caudal medial vestibular nuclei (VeM), (J and K) the caudal mesopallium (MC), (M and N) the dorsomedial thalamus (DTh), and (O and P) the dorsomedial hippocampus (HP). (L) Whole-brain C-FOS counts reveal no difference between the two groups. Bar plots represent the mean \pm SD. C-FOS counts were normalized to the control group. * $P < 0.05$, ** $P < 0.01$; two-tailed t test after Bonferroni correction. Scale bars: 500 μm . FLM, fasciculus longitudinalis medialis; SpV, spinal trigeminal sensory nucleus; L2, field L2; Hy, hypothalamus; AL, ansa lenticularis; MC, caudal mesopallium.

gelatinous cupula and type I and II hair cells flanked by support cells (23). A prerequisite for electromagnetic induction to be viable is the presence of electrosensory molecules in sensory cells (24). To determine whether this is the case, we performed single-cell RNA sequencing on the cristae ampullares using a combinatorial barcoding strategy ($n = 3$ animals). Drawing on the annotated pigeon genome, we obtained 9818 high-quality single cells expressing a median of 3007 genes per cell (Fig. 4A and fig. S8) (25). Unsupervised clustering identified 10 cellular categories, including support cells, dark cells, blood cells, type I, nascent type II, and type II sensory hair cells (26, 27) (Fig. 4B and fig. S9). Using a comprehensive list of 120 voltage-gated ion channels, we screened for voltage-sensitive machinery expressed in hair cell clusters (table S1). Three potassium (K^+) channels ($\text{K}_v1.1$, $\text{K}_v2.2$, and BK) followed by $\text{Ca}_v1.3$ were the most highly expressed voltage-gated ion channels in hair cells (Fig. 4C). We explored whether expression of $\text{Ca}_v1.3$ and K^+ channels would co-cluster in specific subpopulations of sensory cells. This revealed that $\text{Ca}_v1.3/\text{K}_v1.1$ and $\text{Ca}_v1.3/\text{K}_v2.2$ are not coexpressed at high levels across the sensory epithelium ($<5\%$; Fig. 4, D, E, and G). In contrast, coexpression of $\text{Ca}_v1.3$ and BK were enriched in nascent type II and type II hair cells (Fig. 4, F and G). We then asked which cells express the electrosensory isoform of $\text{Ca}_v1.3$ ($\text{Ca}_v1.3_{\text{KKER}}$) (24, 28), focusing on those cells where we could unambiguously determine whether the isoform was present. $\text{Ca}_v1.3_{\text{KKER}}$

was enriched in type II sensory hair cells (33/42 cell IDs, 79%; Fig. 4, H and I), whereas transcripts lacking this exon were predominantly found in nonsensory dark cells (76/81 cell IDs, 94%; Fig. 4, H and I).

Discussion

We have taken a global unbiased approach to characterizing the neuronal circuits that underlie the magnetic sense in pigeons. Using an automated screening method that relies on C-FOS labeling, whole-brain clearing, and light sheet microscopy, we have identified neuronal populations within the pigeon brain that are activated by magnetic fields in the presence and absence of light. In both conditions, we observed C-FOS enrichment within the VeM, which was the sole afferent cranial nerve input station activated by magnetic fields. These data replicate two previous histological studies implicating the vestibular system in the processing of magnetosensory information (4, 13) and strongly suggest that the primary sensors reside in the vestibular epithelia. The persistent activation of the vestibular nuclei by magnetic stimuli in the absence of light demonstrates that the underlying mechanism is not dependent on the formation of light-induced radical pairs. This conclusion is supported by the absence of activation within visual areas, such as the dorsolateral geniculate complex (GLd, thalamofugal), the optic tectum (tectofugal), and the visual Wulst (fig. S3). We further demonstrate that a changing magnetic field is necessary for neuronal

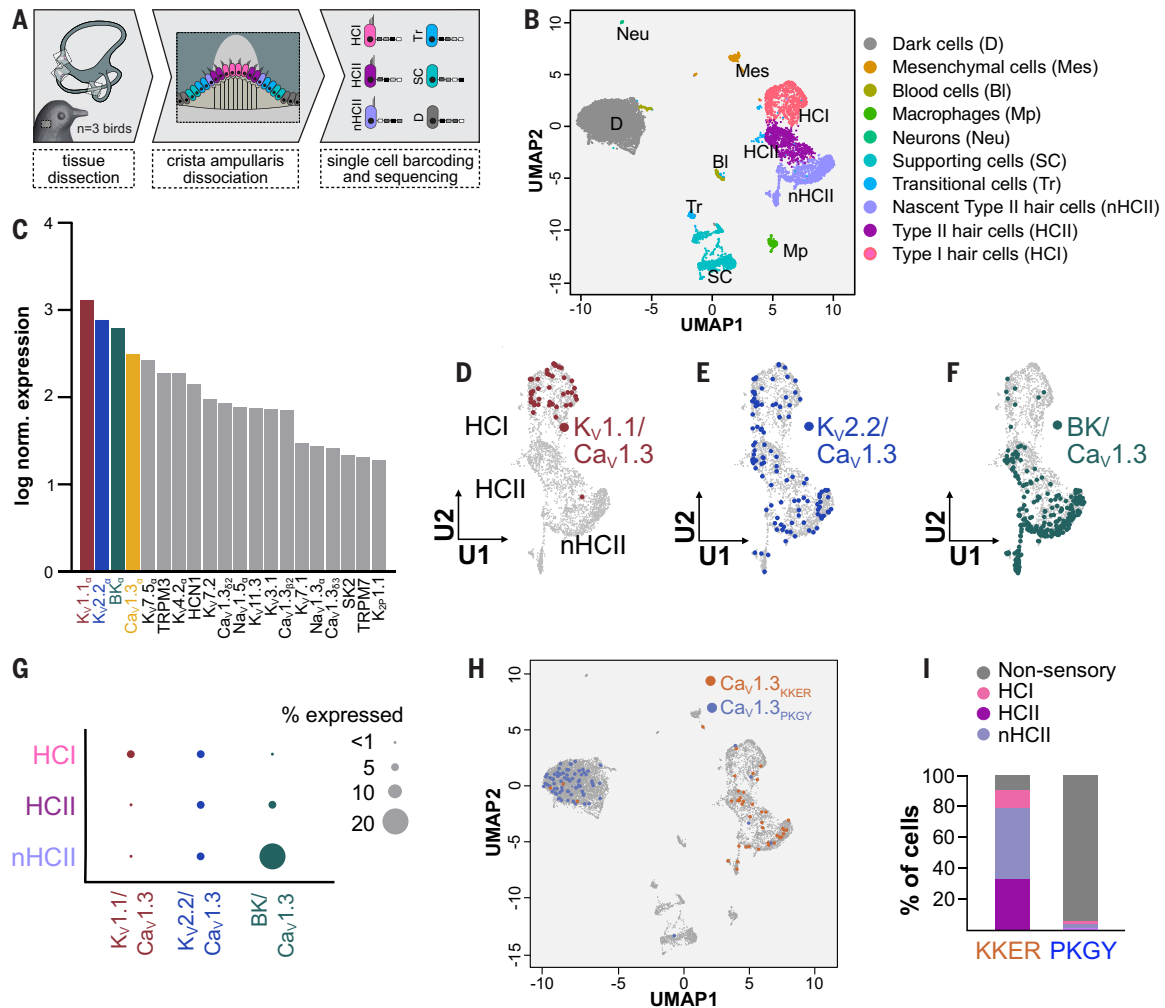


Fig. 4. Electrosensory molecules in the ampullary cristae. (A) Schematic representation of the experimental workflow. Cells from the ampullary cristae ($n = 3$ birds) were dissociated, single cells barcoded, and cDNA libraries sequenced. (B) Uniform manifold approximation and projection (UMAP) representation of 9818 single-cell transcriptomes from the pigeon ampullary cristae, highlighting different cell types. (C) Top 20 voltage-gated ion channels expressed in sensory hair cells. (D to F) Feature plots showing the distribution of hair cells coexpressing (D) Cav1.3/Kv1.1, (E) Cav1.3/Kv2.2, and (F) Cav1.3/BK at high levels (above 75th percentile). (G) Dot plot summarizing the percentages of hair cells coexpressing Cav1.3/Kv1.1, Cav1.3/Kv2.2, and Cav1.3/BK. (H) Expression of Cav1.3 isoforms. The KKER isoform (orange) is expressed predominantly in type II hair cells (HCII) and nascent type II hair cells (nHCII), whereas the PKGY isoform (blue) is found in dark cells. (I) Bar graph showing the distribution of isoforms according to cell type.

activation within the pigeon brain, consistent with a biophysical mechanism that relies on electromagnetic induction.

Our data highlight the importance of several pallial regions in the processing of magnetic information, particularly the mesopallium. This large structure, which shares some functional and molecular homologies with the mammalian claustrum and deep cortical layers, plays an important role in multisensory integration in birds (29). It has been implicated in visual object discrimination (30), imprinting (31), and acoustic processing (32). The mesopallium can be subdivided into six distinct sensory-affiliated subregions and is known to receive input from the thalamus and project to dorsomedial regions of the hippocampus (18). Consistent with our data, magnetically induced neuronal activity has previously been reported in the hippocampus of both pigeons (13) and zebra finches (33). Serving as a spatial memory hub, the hippocampus contains cells that encode an animal's position relative to its environment. In shearwaters (*Calonectris leucomelas*), head direction cells reside within the hippocampus, with increased firing rates associated with a northerly orientation (34). Similarly, in

owls (*Tyto alba*) neurons within the hippocampus and hyperpallium are tuned to flight in an easterly or westerly direction, whereas others encoded the position along the flight path (35). The regions within the hippocampus activated in our light and dark experiments did not overlap, however, it has been shown that visual cues can influence cell mapping in other vertebrates (36). Likewise, the absence of C-FOS enrichment in thalamic regions in our light experiment might be attributable to a masking effect owing to increased input from the visual system via the anterior dorsolateral nucleus of the thalamus (37). Taken together, our data are consistent with a model whereby a light-independent sensor resides within the vestibular system, feeding magnetic information into the mesopallium and hippocampus via a thalamic relay station (Fig. 5, A to C). The exact connectivity of this circuit remains to be defined, and we do not currently understand how magnetic information within pallial regions is encoded. It is conceivable, however, that spatial cells within these regions encode specific components (i.e., inclination, polarity, intensity) of the magnetic vector (38, 39).

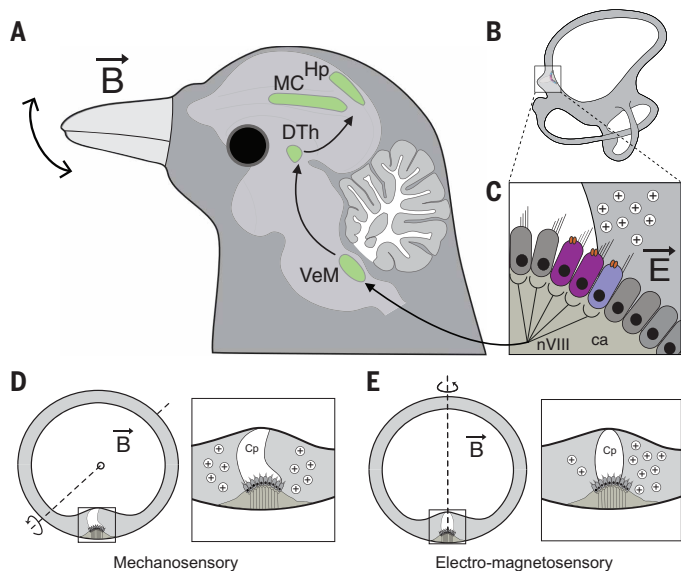


Fig. 5. Model of a magnetosensory circuit driven by electromagnetic induction. (A to C) A changing magnetic field driven by head movement induces an electric field (\vec{E}) in the semicircular canals, which results in a voltage gradient within the endolymph (\vec{B}). Separated by the gelatinous cupula, this difference in charge is detected by type II hair cells, which express the voltage-sensitive calcium channel $Ca_v1.3$ and the large-conductance calcium-activated potassium channel BK. This electromagnetic information is carried from the cristae ampullares (ca) by the vestibulocochlear nerve (nVIII) to the medial vestibular nuclei (VeM), where it is initially processed, before integration with other sensory cues within the mesopallium (MC) and hippocampus (Hp), via a thalamic relay (DTh). (D) Head rotation in the plane of the semicircular canals leads to mechanical stimulation of hair cell stereocilia through displacement of the cupula (Cp) and no induction. (E) In contrast, rotation perpendicular to the plane of the semicircular canal in the presence of a magnetic vector (\vec{B}) results in a redistribution of charge across the cupula without mechanical displacement of hair cells. Consequently, it is possible for the bird to distinguish between mechanical and electromagnetic input.

Because our global analysis of neuronal activity suggests that pigeons rely on a light-independent magnetic sense associated with the vestibular apparatus, we undertook single-cell RNA sequencing of the cristae ampullares. We report high expression levels of voltage-sensitive ion channels known to mediate electroreception ($Ca_v1.3/BK$) (24, 28). Of particular interest was the electrosensory isoform of $Ca_v1.3$, which was preferentially expressed in type II hair cells. Type II hair cells have wide necks and a large apical surface (40), ideal morphological characteristics to detect the electric potential of the endolymph. Previous studies have shown that electric fields generated by pigeon head scanning are within the range of physiological detection of known electrosensory systems (4). It is therefore conceivable that type II hair cells are tuned to detect the redistribution of charge within the endolymph induced by head movement perpendicular to the plane of a semicircular canal in the presence of a static magnetic field. Such movement would not induce deformation of the cupula but nevertheless modulate the activity of hair cells (Fig. 5, D and E) (9). Consequently, a discrete population of projection neurons originating from type II hair cells in the periphery of the cristae ampullares could carry both magnetic and vestibular information, whereas those associated with type I hair cells only encode vestibular input. A subtractive calibration within the central nervous system would then allow the bird to calculate the magnetic vector. An ongoing challenge is to demonstrate both the necessity and sufficiency of specific molecules and cell types for magnetoreception in pigeons. Whereas anatomical lesions of the vestibular system result in severe behavioral

deficits, advances in avian genetics and stem cell technology should permit precise molecular perturbations to test the inductive hypothesis.

REFERENCES AND NOTES

1. J. Shaw *et al.*, *J. R. Soc. Interface* **12**, 0499 (2015).
2. M. Winklhofer, J. L. Kirschvink, *J. R. Soc. Interface* **7** (suppl. 2), S273–S289 (2010).
3. H. Mouritsen, P. J. Hore, *Curr. Opin. Neurobiol.* **22**, 343–352 (2012).
4. S. Nimpf *et al.*, *Curr. Biol.* **29**, 4052–4059.e4 (2019).
5. C. V. Mora, M. Davison, J. M. Wild, M. M. Walker, *Nature* **432**, 508–511 (2004).
6. D. Heyers, M. Zapka, M. Hoffmeister, J. M. Wild, H. Mouritsen, *Proc. Natl. Acad. Sci. U.S.A.* **107**, 9394–9399 (2010).
7. J. Xu *et al.*, *Nature* **594**, 535–540 (2021).
8. T. Hochstoeger *et al.*, *Sci. Adv.* **6**, eabb9110 (2020).
9. R. L. Jungerman, B. Rosenblum, *J. Theor. Biol.* **87**, 25–32 (1980).
10. E. P. Malkemper, S. Nimpf, G. C. Nordmann, D. A. Keays, *J. Exp. Biol.* **223**, jeb232371 (2020).
11. G. C. Nordmann, T. Hochstoeger, D. A. Keays, *PLOS Biol.* **15**, e2003234 (2017).
12. M. Zapka *et al.*, *Nature* **461**, 1274–1277 (2009).
13. L. Q. Wu, J. D. Dickman, *Curr. Biol.* **21**, 418–423 (2011).
14. N. Renier *et al.*, *Cell* **165**, 1789–1802 (2016).
15. T. E. Nichols, A. P. Holmes, *Hum. Brain Mapp.* **15**, 1–25 (2002).
16. G. C. Nordmann *et al.*, *Sci. Rep.* **10**, 915 (2020).
17. J. D. Dickman, Q. Fang, *J. Comp. Neurol.* **367**, 110–131 (1996).
18. Y. Atoji, J. M. Wild, *J. Comp. Neurol.* **520**, 717–741 (2012).
19. N. Lefeldt *et al.*, *J. R. Soc. Interface* **11**, 20140777 (2014).
20. J. M. Wild, *J. Comp. Neurol.* **271**, 451–460 (1988).
21. E. P. Malkemper *et al.*, *Curr. Biol.* **29**, R14–R15 (2019).
22. M. Lauwers *et al.*, *Curr. Biol.* **23**, 924–929 (2013).
23. A. Haque, D. Huss, J. D. Dickman, *J. Neurophysiol.* **96**, 3293–3304 (2006).
24. N. W. Bellono, D. B. Leitch, D. Julius, *Nature* **543**, 391–396 (2017).
25. M. D. Shapiro *et al.*, *Science* **339**, 1063–1067 (2013).
26. M. Scheibinger *et al.*, *Cell Rep.* **40**, 111432 (2022).
27. B. A. Wilkerson *et al.*, *eLife* **10**, e60108 (2021).
28. N. W. Bellono, D. B. Leitch, D. Julius, *Nature* **558**, 122–126 (2018).
29. B. Zarembo *et al.*, *Science* **387**, eadp5182 (2025).
30. W. Clark *et al.*, *Sci. Rep.* **12**, 589 (2022).
31. G. Horn, *Trends Neurosci.* **21**, 300–305 (1998).
32. M. Inda, K. Hotta, K. Oka, *Eur. J. Neurosci.* **53**, 1412–1427 (2021).
33. N. Keary, H. J. Bischof, *PLOS ONE* **7**, e38697 (2012).
34. S. Takahashi, T. Hombe, S. Matsumoto, K. Ide, K. Yoda, *Sci. Adv.* **8**, eabl6848 (2022).
35. A. Agarwal, A. Sarel, D. Derdikman, N. Ulanovsky, Y. Gutfreund, *Proc. Natl. Acad. Sci. U.S.A.* **120**, e2212418120 (2023).
36. M. Geva-Sagiv, S. Romani, L. Las, N. Ulanovsky, *Nat. Neurosci.* **19**, 952–958 (2016).
37. D. Miceli, L. Marchand, J. Repérant, J. P. Rio, *Brain Res.* **518**, 317–323 (1990).
38. L. Q. Wu, J. D. Dickman, *Science* **336**, 1054–1057 (2012).
39. R. N. Shirdhankar, E. P. Malkemper, *Curr. Opin. Neurobiol.* **86**, 102880 (2024).
40. A. J. Ricci, S. L. Cochran, K. J. Rennie, M. J. Correia, *J. Vestib. Res.* **7**, 407–420 (1997).
41. G. C. Nordmann *et al.*, "Data from "A global screen for magnetically induced neuronal activity in the pigeon brain," Dryad (2025); <https://doi.org/10.5061/dryad.0k6djhbd5>.

ACKNOWLEDGMENTS

We thank the core facilities of the IMP Vienna and LMU Munich for their assistance, the graphics department of the IMP Vienna for illustrations, and all members of the Keays lab for discussions and feedback. **Funding:** This work was supported by the European Research Council (D.A.K.: 336725 and 819336); NSERC (S.D.B.); PGSD 557761); Studienstiftung des deutschen Volkes (T.N.K.); and the Max Planck Society (G.C.N. and E.P.M.). **Author contributions:** Conceptualization: G.C.N., S.D.B., T.N.K., E.P.M., L.L., D.A.K.; Methodology: G.C.N., S.D.B., T.N.K., S.N., C.L., M.N.; Investigation: G.C.N., S.D.B., T.N.K., S.N.; Visualization: G.C.N., S.D.B., T.N.K.; Funding acquisition: D.A.K.; Supervision: D.A.K.; Writing – original draft: G.C.N., S.D.B., D.A.K.; Writing – review & editing: All authors. **Competing interests:** The authors declare that they have no competing interests. **Data, code, and materials availability:** The following additional data are publicly available in Dryad (41): the analysis code [ClearMap analysis, permutation-based correction strategy, and single-cell RNA sequencing (scRNA-seq) analysis]; individual C-FOS count matrices for all brains; and scRNA-seq count matrices, marker genes, and raw sequencing reads. **License information:** Copyright © 2026 the authors, some rights reserved; exclusive licensee American Association for the Advancement of Science. No claim to original US government works. <https://www.science.org/about/science-licenses-journal-article-reuse>. This research was funded in whole or in part by the European Research Council (336725, 819336); as required, the author will make the Author Accepted Manuscript (AAM) version available under a CC BY public copyright license.

SUPPLEMENTARY MATERIALS

science.org/doi/10.1126/science.aea6425

Materials and Methods; Figs. S1 to S9; Tables S1 and S2; MDAR Reproducibility Checklist

Submitted 20 July 2025; accepted 4 September 2025; published online 20 November 2025

10.1126/science.aea6425



A global screen for magnetically induced neuronal activity in the pigeon brain

Gregory C. Nordmann, Spencer D. Balay, Thamari N. Kapuruge, Marco Numi, Christoph Leeb, Simon Nimpf, E. Pascal Malkemper, Lukas Landler, and David A. Keays

Science **391** (6790), . DOI: 10.1126/science.aea6425

Editor's summary

We still don't know how pigeons detect the magnetic field of Earth to aid in navigation. To address this conundrum, Nordmann *et al.* used neuronal protein labeling, tissue clearing, and RNA sequencing to investigate the mechanisms, cells, and circuits involved in magnetosensation. Magnetic field stimulation resulted in activation of neurons in the medial vestibular nucleus of the birds' brains. Additional activation was observed in downstream regions, including the dorsal thalamus, mesopallium, and hippocampus. Single-cell RNA sequencing of the cristae ampullaris in the semicircular canals uncovered specialized inner ear hair cells that express ion channels potentially suited for magnetic field detection. These results suggest the existence of special cells within the pigeon forebrain that encode magnetic information and thus facilitate effective navigation. —Peter Stern

View the article online

<https://www.science.org/doi/10.1126/science.aea6425>

Permissions

<https://www.science.org/help/reprints-and-permissions>

Use of this article is subject to the [Terms of service](#)

Science (ISSN 1095-9203) is published by the American Association for the Advancement of Science. 1200 New York Avenue NW, Washington, DC 20005. The title *Science* is a registered trademark of AAAS.

Copyright © 2026 The Authors, some rights reserved; exclusive licensee American Association for the Advancement of Science. No claim to original U.S. Government Works